Seventh Framework Programme
Theme 9 Space FP7-SPA.2009.1.1.02
Monitoring of climate change issues (extending core service activities)

Grant agreement for: Collaborative Project (generic).
Project acronym: **MONARCH-A**
Project title: **MONitoring and Assessing Regional Climate change in High latitudes and the Arctic**
Grant agreement no. 242446
Start date of project: 01.03.10
Duration: 36 months
Project coordinator: Nansen Environmental and Remote Sensing Center, Bergen, Norway

D3.3.2: Modelled time series of surface ocean CO2 partial pressure, air-sea CO2 flux (total, natural, anthropogenic), biological export production, and further biogeochemical variables in relation to climate change and rising atmospheric CO2 for the northern high latitudes and the Arctic and respective changes in marine Arctic carbon budget over the past 50 years (a. with free atmospheric CO2, b. with prescribed atmospheric CO2)

Due date of deliverable: 31.03.2013

Actual submission date: 17.05.2013

Organization name of lead contractor for this deliverable: UiB

Authors: Nadine Goris, Christoph Heinze

Project co-funded by the European Commission within the Seventh Framework Programme, Theme 6 Environment		
Dissemination Level		
PU	Public	
PP	Restricted to other programme participants (including the Commission)	X
RE	Restricted to a group specified by the consortium (including the Commission)	
CO	Confidential, only for members of the consortium (including the Commission)	

ISSUE	DATE	CHANGE RECORDS	AUTHOR
0	08/04/2011	Template	K. Lygre
1	17/05/2013	1st version	N. Goris, C. Heinze

SUMMARY

Two marine carbon cycle hindcasts were carried out with the stand-alone coupled physical-biogeochemical ocean model MICOM-HAMOCC-M. Both model runs are based on the evaluated spin-up integration of 800 years as described in D3.3.1, but they differ in the way atmospheric CO_2 is treated. While the first run uses prescribed atmospheric CO_2 concentrations (run CONC), the second runs uses prescribed atmospheric CO_2 emissions, allowing a feedback of the oceanic CO_2 uptake (run EMIS).

In order to compare the data-products of WP3.1 and WP3.2 with the model output in the Arctic, run CONC is primarily considered since it supplies a more realistic CO_2-forcing. Run EMIS is additionally considered for analysing the oceanic CO_2-uptake in the Arctic.

Run CONC show very good agreement with the data-sets for pCO_2, primary production, temperature and salinity; especially in the Nordic Seas. Due to low availability of data for nitrate, phosphate, silicate, alkalinity, and dissolved inorganic carbon, the model can only be validated for Station M; here the model performs well. Based on these promising results, the modelled trends for the last 50 years are analysed. Temperature, salinity, dissolved inorganic carbon, alkalinity, silicate, and oceanic pCO_2 show positive trends in the GIN seas. Trends north of 75°N are difficult to establish due to melting ice cover (associated with changing trends within the last 50 years) and missing data. Collectively, the arctic CO_2-uptake is steadily increasing within the last 50 years, while the CO_2-uptake in the GIN seas is stagnating for the last ten years. This alarming finding is confirmed by the results of run EMIS.

The data of both model simulations are stored as netCDF-files on two external external hard drives at the Geophysical Institute of the University of Bergen and amount altogether to 1 Terabyte. Please contact Nadine Goris (nadine.goris@gfi.uib.no) for further information.

MONARCH-A CONSORTIUM

Participant no.	Participant organisation name	Short name	Country
1 (Coordinator)	Nansen Environmental and Remote Sensing Center	NERSC	NO
2	The University of Sheffield	USFD	UK
3	Universität Hamburg	UHAM	NO
4	Centre National de la Recherche Scientifique	CNRS	FR
5	Scientific foundation Nansen International Environmental and Remote Sensing Center	NIERSC	RU
6	Universitetet i Bergen	UiB	NO
7	Danmarks Tekniske Universitet	DTU	DK
8	Institut Francais de Recherche pour l'Exploitation de la Mer	IFREMER	FR

Table of Contents

Table of Contents 5

1 Introduction 8

2 Description of employed model runs and data sources..... 9

3 Modelled timeseries 10

3.1 Changes in surface-water and atmospheric partial pressure of CO_2 and their effect on the oceanic CO_2 uptake 10

3.1.1 Surface-water partial pressure of CO_2 (pCO_2^{sea}) 10

3.1.2 Atmospheric partial pressure of CO_2 (pCO_2^{air}) 13

3.1.3 Oceanic CO_2 uptake 14

3.2 Changes in primary production and suspended calcium carbonate 16

3.2.1 Integrated Primary Production 16

3.2.2 Suspended Calcium Carbonate 18

3.3 Changes in the physical variables salinity and temperature 20

3.4 Changes in the biogeochemical variables dissolved inorganic carbon, alkalinity, nitrate, phosphate, silicate, and oxygen 23

4 Summary 25

5 References 27

List of Figures

Figure 1: Number of months with LDEO/SOCAT data-coverage per MICOM-HAMOCC-M grid-cell for 1972-2011.....10

Figure 2: Temporal Correlations and Biases of the pCO_2^{sea} data-model-comparison between the data-product SOCAT-LDEO and the model MICOM-HAMOCC-M for 1972-2011....11

Figure 3: Annual pCO_2^{sea} cycle of data-product SOCAT-LDEO and model MICOM-HAMMOC-M in 2007 for two different grid points.....11

Figure 4: Selected pCO_2^{sea} Timeseries for 1961-2011 as modelled by MICOM-HAMOCC-M (including SOCAT/LDEO-Observations).....12

Figure 5: pCO_2^{sea}-Trend for 1961-1986 and for 1986-2011 as modelled by MICOM-HAMOCC-M 12

Figure 6: Monthly pCO_2^{atm} Correlations and Biases of the spatial distribution for data product/model forcing for 1972-2011 13

Figure 7: Selected pCO_2^{atm} Timeseries for 1961-2011 as modelled by MICOM-HAMOCC-M (including GLOBALVIEW-records) 14

Figure 8: Oceanic CO_2-uptake for run CONC and run EMIS....15

Figure 9: Number of months with SeaWiFs-Primary Production data-coverage per MICOM-HAMOCC-M grid-cell for the time period 1998-2010 16

Figure 10: Temporal Primary Production Correlations of the data-model-comparison between the data-product SeaWiFs and the model MICOM-HAMOCC-M for 1998-2010 17

Figure 11: Selected Primary-Production-Timeseries for 1998-2010 as modelled by MICOM-HAMOCC-M (including SeaWiFs-retrievals) 17

Figure 12: Primary Production-Trend for 1961-2011 and for 1998-2011 as modelled by MICOM-HAMOCC-M....18

Figure 13: Number of months with MODIS-Suspended Inorganic Carbon data-coverage per MICOM-HAMOCC-M grid-cell for the time period 2002-2010 19

Figure 14: Temporal Correlations of the data-model-comparison between the data-product MODIS and the model MICOM-HAMOCC-M for the time period 2002-2010....19

Figure 15: Number of months with SST and SSS data-coverage per MICOM-HAMOCC-M grid-cell for the time period 1972-2011 20

Figure 16: Monthly Correlations, Biases and Root Mean Square Errors of the spatial SSS/SST-distribution for data product/model output for 1972-2011....20

Figure 17: Temporal SST/SSS-correlations of the data-model-comparison between the data-product LDEO-SOCAT-GLODAP-CARINA-Station M and the model MICOM-HAMOCC-M for the time period 1972-2011....21

Figure 18: Selected SSS/SST-Timeseries for 1961-2011 as modelled by MICOM-HAMOCC-M (including SOCAT/GLODAP/Station M-records) 21

Figure 19: 50-year Trends (1961-2011) of Temperature and Salinity in two different depth levels as modelled by MICOM-HAMOCC-M 22

Figure 20: Number of months with phosphate surface data per MICOM-HAMOCC-M grid-cell and temporal correlations of the associated data-model-comparison for 1972-2011 23

Figure 21: Selected Nitrate/ Phosphate/ Silicate/ DIC/ Alkalinty-Timeseries for 2001-2008 as modelled by MICOM-HAMOCC-M (including Station M-data).....24

Figure 22: 50-year Trends (1961-2011) of Phosphate, Nitrate, Silicate, Alkalinity and Dissolved Inorganic Carbon (DIC) as modelled by MICOM-HAMOCC-M 24

List of Tables

Table 1: Arctic data-availability of all considered variables for the time-period 1960-2010....25

1 Introduction

For the high latitudes, a thorough monitoring of the marine carbon cycle is important, as the general "polar amplification" of climate change also translates into the biogeochemical realm. As compared to the global ocean, the sink for human-produced CO_2 is fairly small in the Arctic Ocean itself (e.g., *Lundberg and Haugan, 1996*) and of intermediate importance in the Greenland-Iceland Sea (e.g., *Jeansson et al., 2011*), in any case much less relevant than the Southern Ocean sink in total (e.g., *Tjiputra et al., 2010b*). Nevertheless, it is important to follow up this Arctic sink as a further control of regional carbon budgets (as relevant for control of emission reduction goals for specific nations/regions) and to record changes in nutrient/cycling and biological carbon cycling on the way towards a "*blue Arctic*". Especially interesting is the change in carbon uptake due to the high solubility of CO_2 at low temperatures (*Weiss, 1974*), but on the other hand low buffer capacity for excess CO_2 (*Sabine et al., 2004*). Uptake reductions due to rising CO_2 partial pressure in Surface Ocean and atmosphere will lead to a potentially accelerated decrease in ocean CO_2 uptake in the Arctic. Such a trend will, however, also depend on the development of the sea ice cover, of the hydrography (temperature, salinity), and the deep-water production mode (potentially away from shelf-plume induced deep-ventilation to more open ocean ventilation, see e.g. *Aagaard et al., 1985*). Any change in air-sea CO_2 flux will also alter the atmospheric CO_2 concentration and hence the radiative budget of the atmosphere through the greenhouse effect. Due to the feedbacks between climate change and the carbon cycle and between rising CO_2 itself, the carbon cycle needs to be included in monitoring as well as prediction of climate change.

The decrease in Arctic Ocean buffer capacity has its corresponding counterpart in strongly enhanced ph-reduction and carbonate-saturation reduction in the ocean surface layer at cold temperatures (e.g., *Orr et al., 2005; Steinacher et al., 2009*). During the past million years, the saturation for aragonite (the metastable polymorph of calcium carbonate $CaCO_3$) and for calcite (the less soluble $CaCO_3$ polymorph) has never become negative (undersaturation) (e.g., *Caldeira and Wickett, 2003*). This changes now quickly, and the first appearance of aragonite undersaturation is projected already for year 2016 (*Steinacher et al., 2009*). This progressing ocean acidification can potentially have severe impacts on marine ecosystem functioning. Especially, *pteropods* (small snails which produce aragonitic shell material) may be affected as well as cold water corals (e.g. *Guinotte and Fabry, 2008*), which both have important roles in the marine foodweb. Potential regional extinction of marine key species together with a projected decrease in oceanic primary (plant) production (e.g. *Steinacher et al., 2010*) can have severe implications for the standing stock biomass in the ocean and respective food production also for human societies.

It would be desirable to measure a series of multi-tracer variables in the ocean in order to follow-up the changing carbon cycle. We are still far away from such capabilities. In order to make at least an attempt, we combine model results and data-products to identify trends in key variables of the marine carbon cycle.

2 Description of employed model runs and data sources

For the integration of the produced-data sets with the biogeochemical model hindcasts, the model MICOM-HAMMOC-M was deployed. It is based on the MICOM-HAMOCC version described in *Assmann et al., 2010*, but newly integrated in the NorESM framework. NorESM is a state-of-the-art Earth system model originating from the Community Climate System Model 4. It differs from the CCSM4 in the ocean component (MICOM), the ocean carbon cycle (HAMOCC) and the treatment of atmospheric chemistry, aerosol and clouds. In order to adapt MICOM-HAMOCC to NorESM, the north pole of the model was shifted from Siberia to Greenland. Moreover, the model resolution was refined, so that two model versions are now available: MICOM-HAMOCC-L (3.6° resolution) and MICOM-HAMOCC-M (1.125° resolution). Since the finer resolution is advantageous for the data-model comparison of MONARCH-A, MICOM-HAMOCC-M is deployed here. The synoptically forced coupled physical biological ocean model run is based on a spin-up integration of 800 years with a constant preindustrial atmospheric CO_2 concentration of 278 ppm, initialised with climatology-data from the World Ocean Atlas (WOA). Two marine carbon cycle hindcasts were carried out differing in the way atmospheric CO_2 is treated. While the first run uses prescribed atmospheric CO_2 concentrations (run CONC), the second runs uses prescribed atmospheric CO_2 emissions, allowing a feedback of the oceanic CO_2 uptake (run EMIS).

Relevant Earth Observations data-sets have be exploited and reprocessed to build compatible arctic data-sets for the ECVs of the marine carbon cycle (oceanic and atmospheric pCO_2 as well as ocean colour/primary productivity). In detail, for oceanic pCO_2 the comprehensive data-sets SOCAT and LDEO have been combined leading to 796.666 point observations north of 60^o latitude in the period 1972-2011. Observations of atmospheric CO_2 were collected from the GLOBALVIEW-CO2 data integration project comprising 8 measurement stations north of 60^o latitude with continuous extended records of CO_2 in the period 1979-2011. Monthly Primary Production fields were retrieved from the sensors MODIS and SeaWiFs. The data-product is available for different kinds of chlorophyll retrieving algorithms and Primary Production retrieving algorithms for the time period 1998-2010 (June-September) for the pelagic arctic area at a spatial resolution of 4 km. The MODIS sensor was furthermore utilized for the retrieval of monthly concentrations of Emilia huxleyi, coccoliths, diatomic chl and suspended inorganic carbon produces by Emilia huxleyi for the time period 2002-2010 (June-September) for the Arctic. Furthermore, the datasets GLODAP, CARINA and Station M are considered to allow for a data-product for dissolved inorganic carbon, alkalinity, nitrate, silicate, and phosphate. It contains of 8.362 Arctic surface level observations for the period 1972-2009. Finally, both temperature and salinity are included in most of the data-sets (namely SOCAT, LDEO, GLODAP, CARINA and Station-M), so that 810.276 temperature observations and 686.844 salinity observations could be extracted for the Arctic.

In order to compare the data-products with the model output in the Arctic, run CONC is primarily considered since it supplies a more realistic CO_2-forcing. Run EMIS is additionally considered for analysing the oceanic CO_2-uptake in the Arctic (*see Section 3.1.3*).

3 Modelled timeseries

3.1 Changes in surface-water and atmospheric partial pressure of CO_2 and their effect on the oceanic CO_2 uptake

3.1.1 Surface-water partial pressure of CO_2 (pCO_2^{sea})

The data-set used for the model-observation comparison combines the Global Surface pCO_2 LDEO Database (*Takahashi et al., 2012*) with the Surface Ocean Carbon Atlas (SOCAT) Database (*Pfeil et al., 2012*). Both databases are unique in terms of coverage and quantity of quality controlled observations of pCO_2/fCO_2. While the LDEO database consists of approximately 6.4 million quality controlled measurements of surface water pCO_2 made over the global oceans during 1957-2011, the SOCAT database includes fCO_2 data from more than 10 countries, producing an initial database composed of more than 1850 cruises from 1968 to 2007 with approximately 6.3 million measurements. Within the SOCAT dataset the fCO_2 measurements from an autonomous Neill underway pCO2 system onboard R/V G.O.Sars (utilised in WP3.2) are included.

For the combined SOCAT/LDEO dataset, all data north of 60°N from both SOCAT and LDEO were included. Before integrating the selected SOCAT data, the fCO_2 data from the SOCAT database were converted into pCO_2 data following the conversion formula of *Takahashi et al, 2012*. Finally the combined dataset consists of 796.666 pCO_2 data points north of 60° latitude in the period 1972-2011, thereof 671.278 SOCAT measurements (covering the time period 1981-2011 in the Arctic) and 125.388 LDEO measurements (covering the time period 1972-2008 in the Arctic). The data was interpolated to the MICOM-HAMOCC-M grid, leading to a maximum of 46 month with observation for one grid cell within the time period 1972-2011. Figure 1 shows that this number of 46 month is an exception. While a few grid cells have data-coverage of over 20 month, most of the grid cells have data-coverage of less than 6 month and half of the oceanic arctic grid cells have no coverage at all. Due to this weak data-coverage a confident analysis of model performance and pCO_2 trends is difficult to achieve.

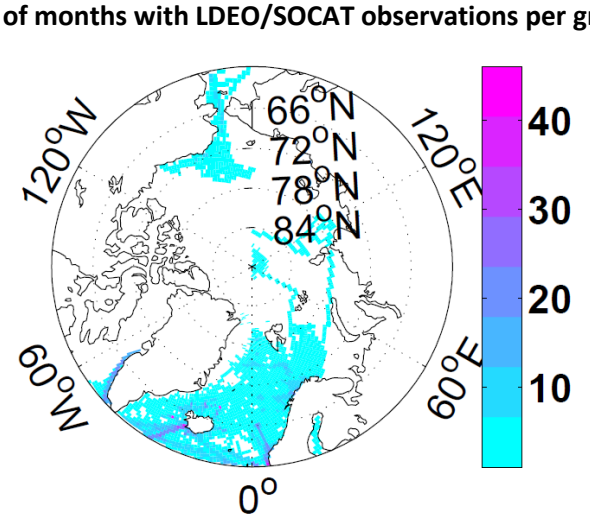

Figure 1: Number of months with LDEO/SOCAT data-coverage per MICOM-HAMOCC-M grid-cell for 1972-2011.

Comparing the time series per grid point with the data-product it can be seen that the model reproduces the temporal behaviour of the data well south of 66°N, between 60°W and 30°E with good correlations and moderate biases (*see Figure 2*). In the areas between 30°E and 145°E and between 180°W and 150°W the data/model comparison shows large biases and mixed correlations. Both areas are characterized by sparse and only very recent observations (starting 1999) leading to a large uncertainty in the initialization of the model. The mixed correlations but moderate biases in the area north of 66°N, between 60°W and 30°E can be explained by the differences in the annual cycles of model and data. Here, the pCO_2 concentration of the model has its low point in June and increases afterwards, while the pCO_2-data shows low points in both June and August and only afterwards an increasing pCO_2 concentration. Due to the sparsity of the data north of 66°N, the data-points can highlight this negative summer feature (by having observations in months with differing model/data behavior) or ignore it (no observations in month with differing behavior), leading to grid cells with positive correlations directly next to grid cells with negative correlation (*see Figure 3*).

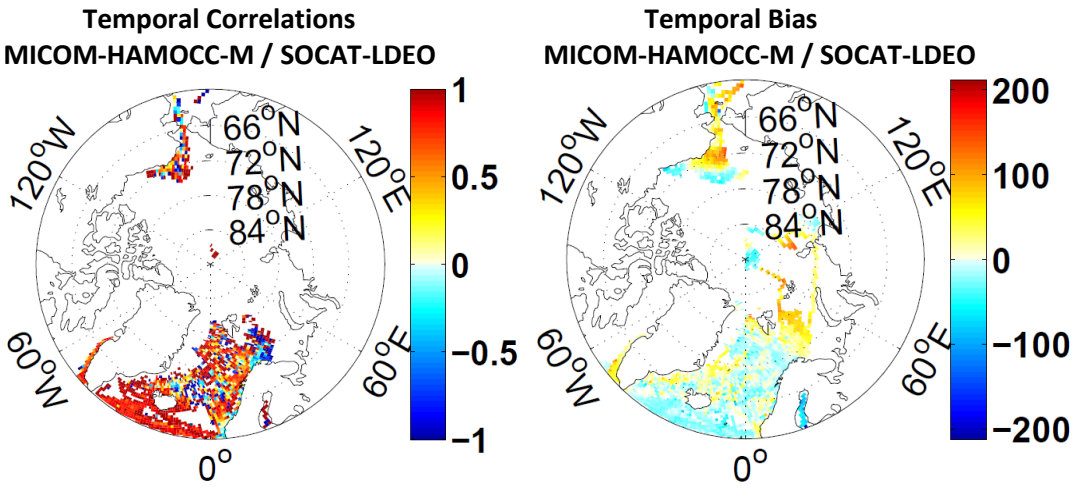

Figure 2: Temporal Correlations (left) and Biases (right) of the pCO_2^{sea} data-model-comparison between the data-product SOCAT-LDEO and the model MICOM-HAMOCC-M for 1972-2011.

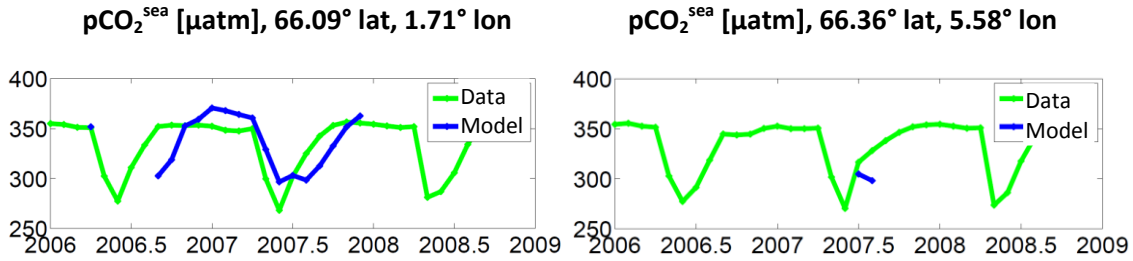

Figure 3: Annual pCO_2^{sea} cycle of data-product SOCAT-LDEO (blue) and model MICOM-HAMMOC-M (green) in 2007 for two different grid points. The pictures illustrate how the low availability of data can lead to negative correlations (right panel) and positive correlations (left panel) in adjoined grid cells.

The timeseries for oceanic pCO_2 at different coordinates (*see Figure 4*) shows the consistency of the variable with a relative regular annual cycle and a positive trend for all coordinates for model and data. The complete modelled trend for the area north of 60°N is illustrated in Figure 5.

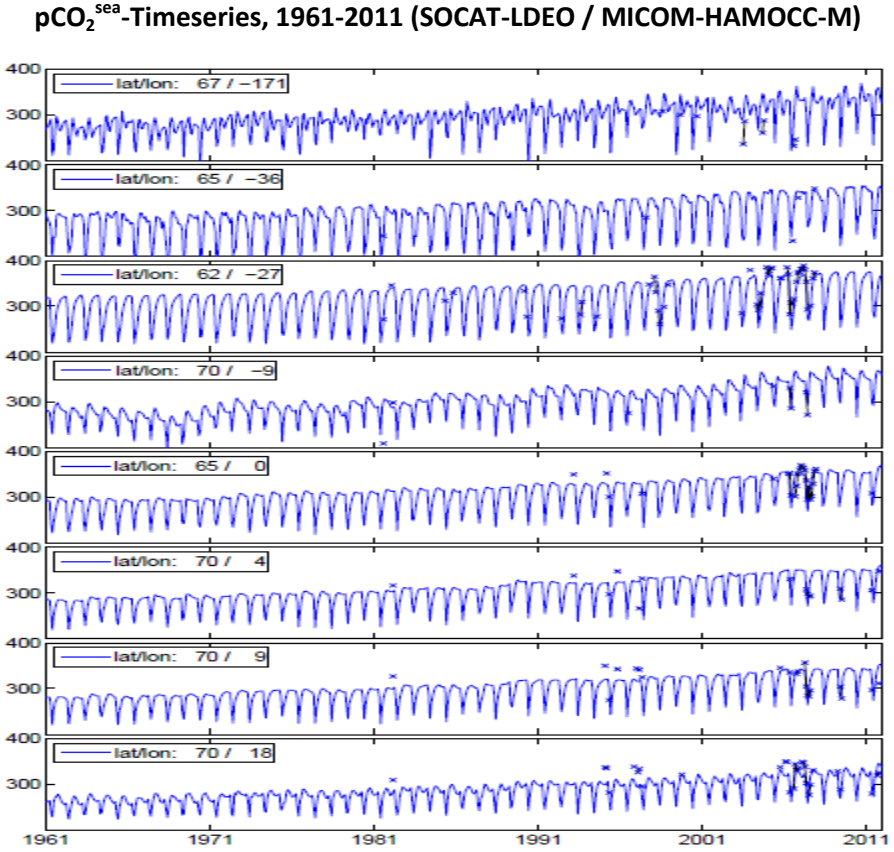

Figure 4: Selected pCO_2^{sea} Timeseries and for 1961-2011 as modelled by MICOM-HAMOCC-M (blue lines). SOCAT/LDEO-Observations are marked by blue crosses and black lines. Associated offsets and coordinates are denoted in the right panel.

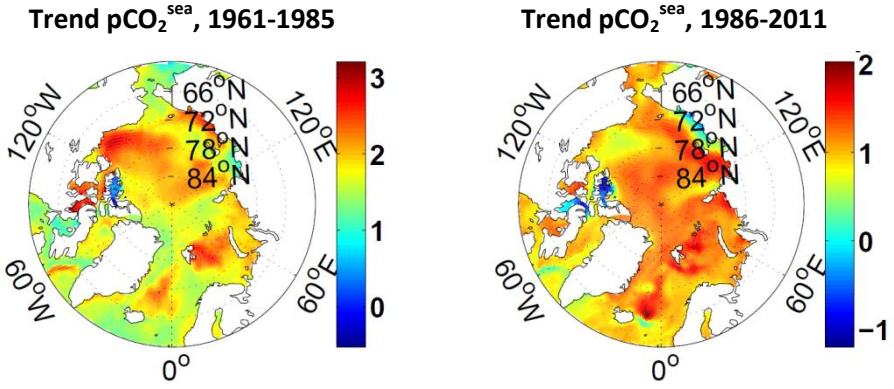

Figure 5: pCO_2^{sea}-Trend for 1961-1986 (left panel) and for 1986-2011 (right panel) as modelled by MICOM-HAMOCC-M.

The new combination of the SOCAT/LDEO datasets made a more comprehensive picture of pCO_2 in the Arctic possible, showing that the model MICOM-HAMOCC performs wells in the region between 60°W and 30°E. Nevertheless even the combination of LDEO/SOCAT does not give a comprehensive picture of pCO_2 in the remaining areas. Here, measurements are spare and very recent (after 1999) and moreover mainly sampled in August/September. Due to this feature no full annual cycle is available, making a significant comparison impossible. Regular observations are a necessity in this area, so that trends and annual cycles can be estimated.

3.1.2 Atmospheric CO_2 partial pressure (pCO_2^{air})

Observations of atmospheric CO_2 were collected from the GLOBALVIEW-CO2 data integration project (*GLOBALVIEW-CO2, 2011*) comprising 8 measurement stations north of 60° latitude with continuous extended records of CO_2. Thereby each of the chosen measurement stations provides at least 7 years of observations with up to 32 years of observations. Their extended records comprise smoothed values as well as interpolated and extrapolated values defined for each month in the period 1979-2011 leading to 384 months covered with extended records for each station and hence 3072 data points. Combining the extended records of atmospheric CO_2 with atmospheric pressure and water vapour pressure, atmospheric pCO_2 can be estimated. Since there are no continuously observed water vapour fields, the water vapour has to be calculated from SOCAT-values of salinity and temperature (here, SOCAT is the data-product of choice since atmospheric pressure is not included in the LDEO database). Due to the low availability of data it is very difficult to achieve a confident estimate for water vapour pressure and atmospheric pressure at the coordinates of the measurement stations, especially for the whole period 1979-2011. As a first approximation, it is here therefore assumed that atmospheric pCO_2 equals the atmospheric CO_2 concentration. This approach is consistent with the forcing of the model which utilizes the same approximation.

Looking at the statistics of the data/model-comparison, the forcing of the model produces the temporal behaviour of the data-product well with correlations better than 0.8 and biases less than 10 ppm (in absolute value) for every station. Nevertheless, the illustration of the monthly biases of the spatial distribution (*see Figure 6*) shows that the amplitude of the annual cycle of the model is in general smaller than the amplitude of the data product. Besides this difference in amplitude there is very good agreement between spatial distribution of data product and model with correlations better than 0.96.

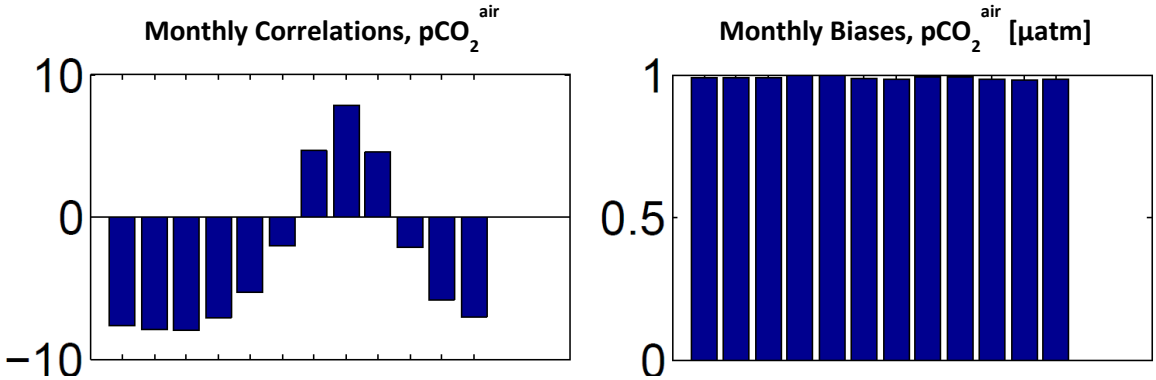

Figure 6: Monthly pCO_2^{atm} Correlations and Biases of the spatial distribution for data product/model forcing for 1972-2011. Monthly Biases show that the amplitude of the annual cycle of the model forcing is smaller than the one of the data-product.

pCO_2^{atm}-Timeseries, 1961-2011 (GLOBALVIEW / MICOM-HAMOCC-M)

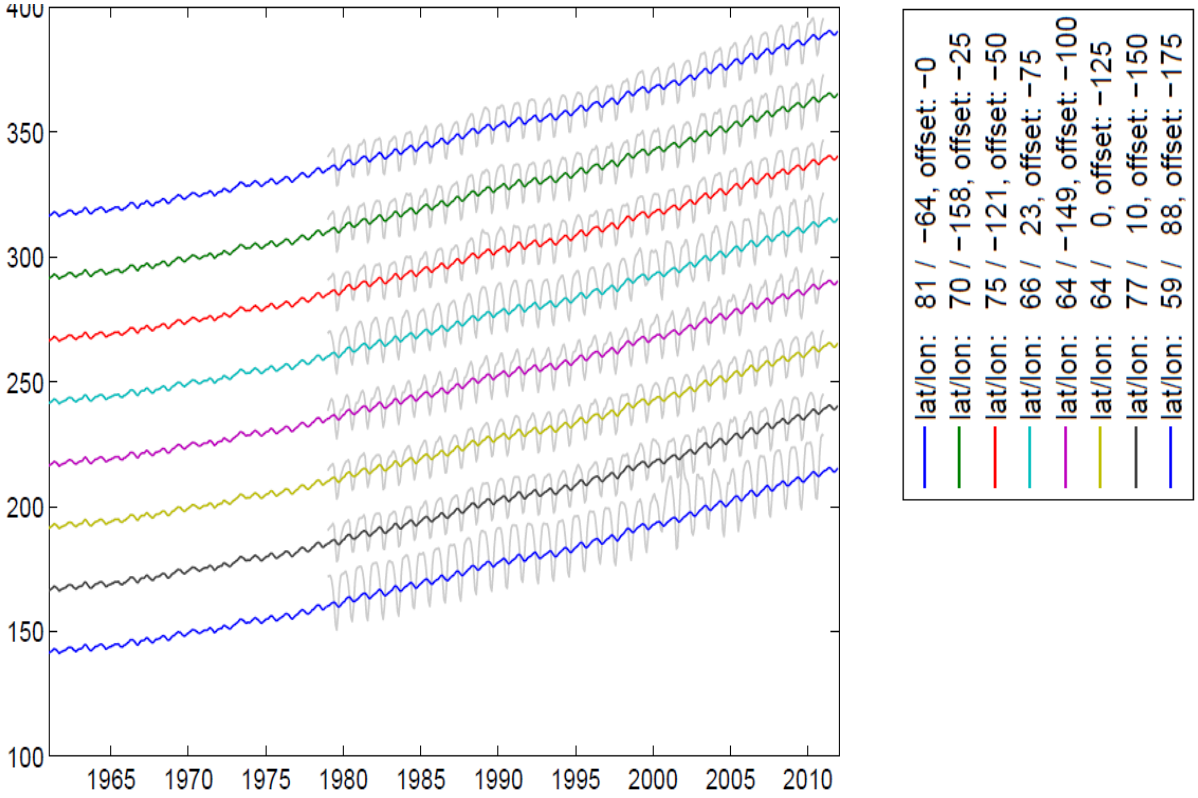

Figure 7: Selected pCO_2^{atm} Timeseries for 1961-2011 as modelled by MICOM-HAMOCC-M (colored lines). Extended GLOBALVIEW-records are marked by black lines. Associated offsets and coordinates are denoted in the right panel.

For a relatively uniform variable like CO_2^{atm} (characterised by a regular annual cycle and a similar temporal evolution for adjacent grid points), the GLOBALVIEW-CO_2 dataset shows in an impressive way that continuous measurements at a fixed coordinate are by far more important than a large amount of widespread observations. The 8 measurement stations of CO_2^{atm} give a comprehensive picture of the development of CO_2^{atm} for the period of 1979-2011 and validate the CO_2-forcing of the model. The latter has a positive trend of 1.176 ppm for 1961-1986 and 1.72 ppm for 1986-2011.

3.1.3 Oceanic CO_2 uptake

Considering run CONC (which is also considered in Sections 3.1.1 and 3.1.2), the globally averaged CO_2 uptake shows a stronger increase than the averaged Arctic uptake (*see Figure 8*). Splitting the Arctic CO_2 uptake into CO_2 uptake of the GIN seas and CO_2 uptake of the remaining Arctic basin, it can be seen that there is a significant slow-down of the uptake of the GIN seas in the last 10 years, while this feature cannot be find in the remaining basin. This slowdown is probably caused by the warming sea surface temperature and increasing salinity in the GIN seas, while the process of sea ice melting counters the warming sea surface temperatures in the remaining Arctic basin. These findings are confirmed by run EMIS (*see Figure 8*). The relatively smooth uptake-curves of run EMIS are

caused by the fact that the atmospheric CO_2 emissions experience no land-uptake causing a relatively weak annual cycle of atmospheric CO_2.

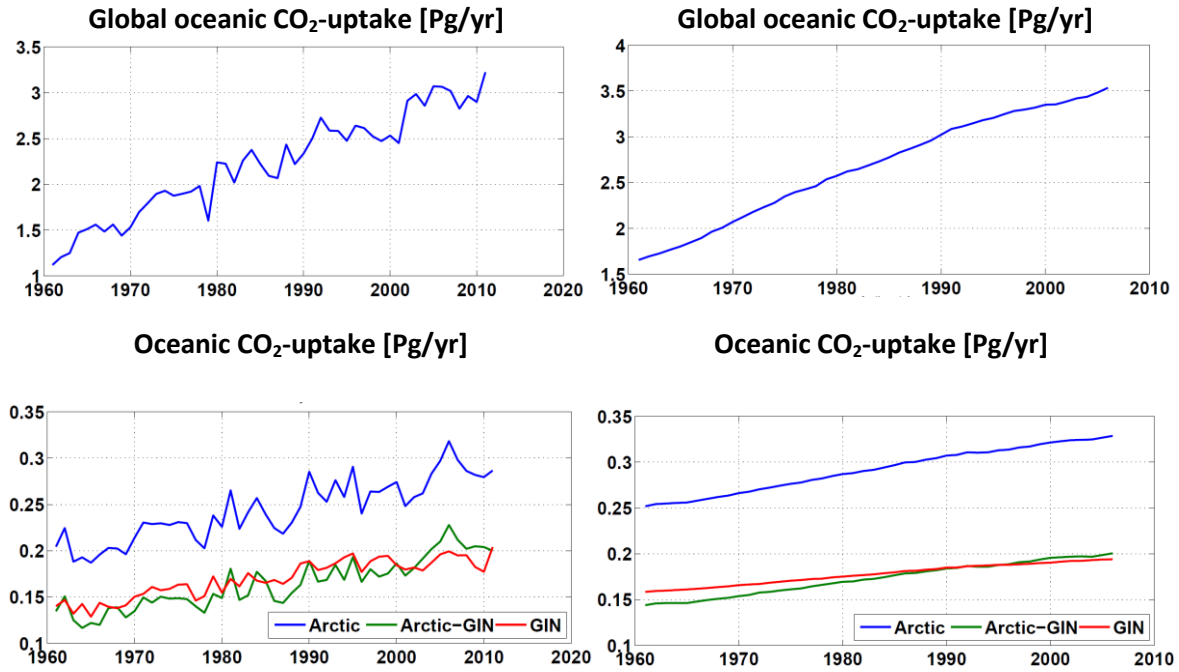

Figure 8: Oceanic CO_2-uptake for run CONC (left panels) and run EMIS (right panels). Here, the upper panels illustrate the globally averaged CO_2-uptake, while the lower panels illustrate the CO_2-uptake for different Arctic regions.

The uptake rates of both runs are in very good agreement with the results of *Jeansson et al.,2011* which report an air-sea flux of 0.19 Gt yr^{-1} (Gt=Pg) for the GIN Seas.

3.2 Changes in primary production and calcium carbonate

3.2.1 Primary Production

Monthly Primary Production fields were retrieved from the sensors MODIS and SeaWiFs. For both sensors, 3 colour data sources were investigated, retrieved with either the standard NASA OC3/4 retrieval algorithm (spatial resolution: 4km for MODIS and 9km for SeaWiFS) or the NASA GSM retrieval algorithm (spatial resolution: 4km for MODIS and 9km for SeaWiFS) or the NASA GSM algorithm combined with a procedure of cloudiness partial removal from the Oregon State University data (spatial resolution: 9km). Furthermore, three different algorithms for the retrieval of Primary Production were tested for the Arctic Basin, namely the algorithms of *Behrenfeld et al., 1997*, *Behrenfeld et al., 2005,* and *Marra et al., 2003*. Since the combination of the retrieval from the Oregon State University together with the Behrenfeld algorithm showed the best results for the Primary Production retrieval (in comparison with shipborne Primary Production measurements at stations across the Arctic Basin, see *Petrenko et al., 2012*), the associated dataset from the SeaWiFs sensor is utilized for the data/model comparison. This dataset is available for the time period 1998-2010 (June-September) leading to a maximum of 48 month with observation for one MICOM-HAMOCC-M grid cell. Smaller numbers of observation-months are resulting from cloudiness and ice cover (*Petrenko et al., 2013; see Figure 8*). Since ice cover of model and data-product differ, all grid points which show different ice-cover than the data-product are taken out of the comparison for the respective point in time.

Number of months with observations of Primary Production per grid point

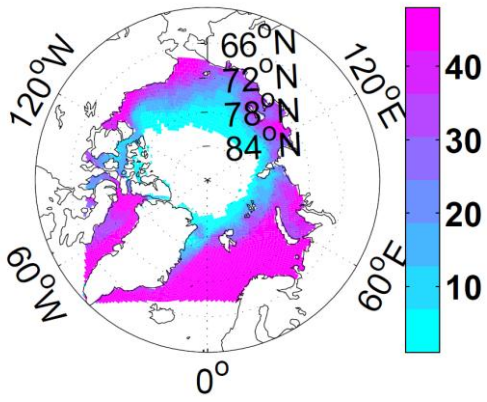

Figure 9: Number of months with SeaWiFs-Primary Production data-coverage per MICOM-HAMOCC-M grid-cell for the time period 1998-2010.

Looking at the correlations of the temporal comparison per grid point (*see Figure 9*) it can be seen that the model reproduces the temporal behaviour of Primary Production well. Correlations of exactly 1.0 or -1.0 are due to the low availability of data. Biases are as well moderate except for relatively high biases at the northern Greenland coast and the Russian coast section at the Barents Sea. Nevertheless, monthly correlations are only moderate showing that the model is able to produce the general temporal behaviour, but not the monthly trend (*see Figure 10*). This is due to the fact that the model is not able to produce the exact height of the annual Primary Production peak. Selected timeseries for different coordinates confirm that the model produces the general behaviour of Primary Production well, but is not able to reproduce monthly trends (*see Figure 11*).

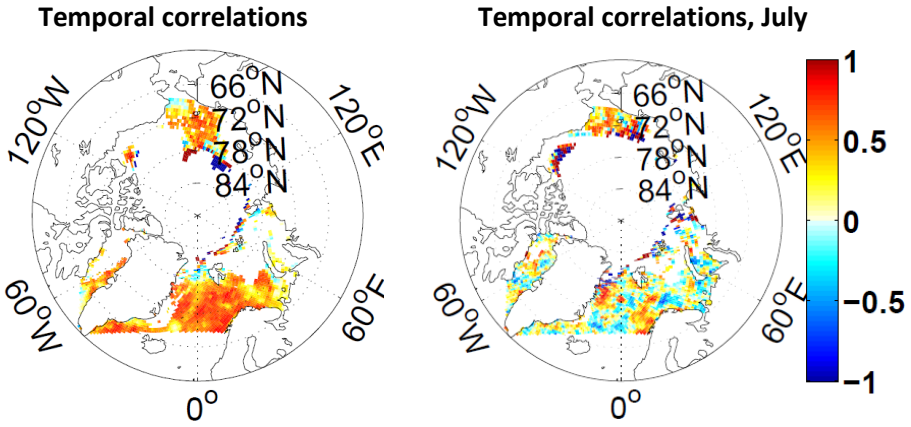

Figure 10: Temporal Primary Production Correlations of the data-model-comparison between the data-product SeaWiFs and the model MICOM-HAMOCC-M for the time period 1998-2010 (left panel: correlations for the whole time period, right panel: correlations for July only).

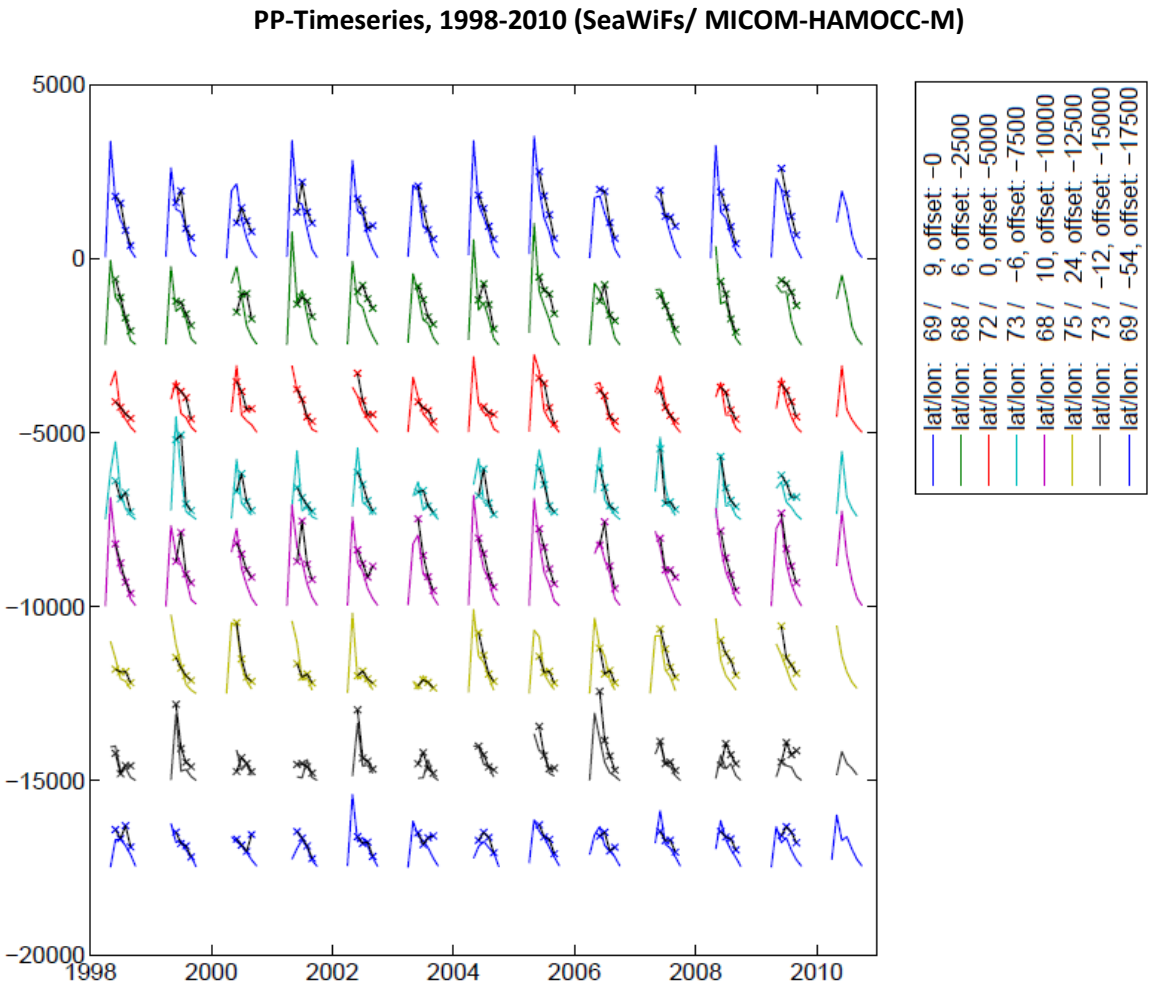

Figure 11: Primary Production: Selected Timeseries for 1998-2010 as modelled by MICOM-HAMOCC-M (colored lines). SeaWiFs-Observations are marked by colored crosses and black lines. Associated offsets and coordinates are denoted in the right panel.

The timeseries show furthermore that the annual cycle of Primary Production is irregular in both range and form. For relatively short timescales like the period 1998-2010, it is therefore very likely that the calculated linear trend is governed by just a few extreme values which are not representative for a general trend in Primary Production. The relatively low values of the modelled trends for the time period 1961-2011 (*see Figure 12*) support this thesis. Significant positive trends within the last 50 years can only be confirmed for the region north of Greenland (*see Figure 12*).

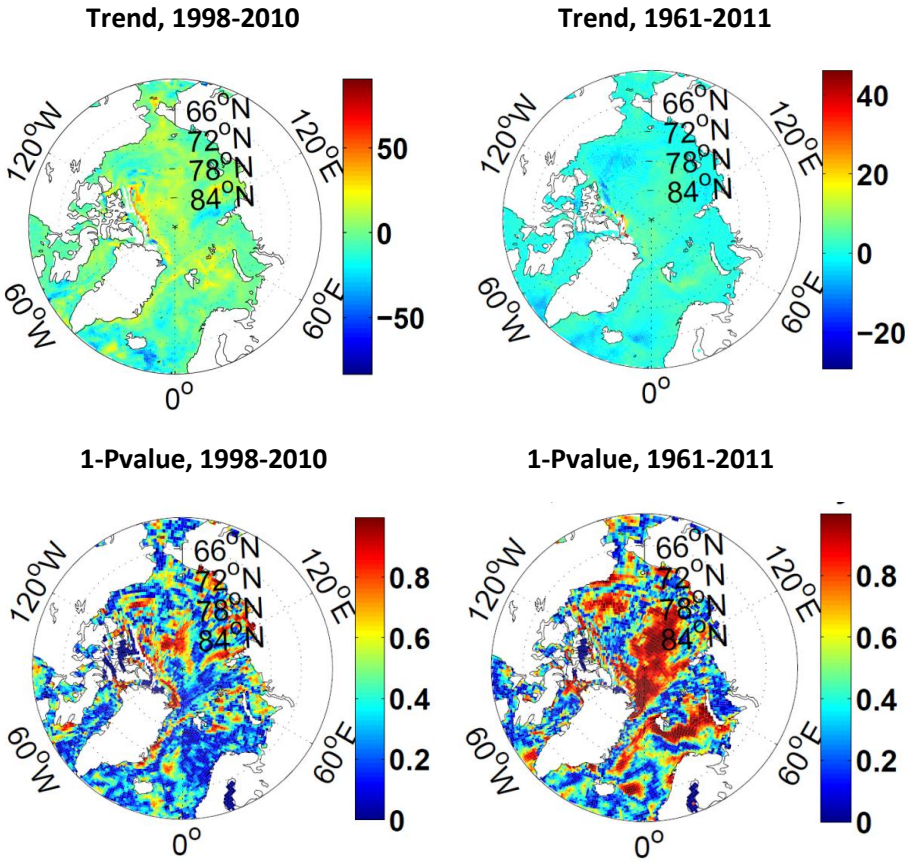

Figure 12: Primary Production-Trend and associated P-values for 1961-2011 (left panel) and for 1998-2011 (right panel) as modelled by MICOM-HAMOCC-M. A trend is considered significant if 1-Pvalue > 0.95 holds.

3.2.2 Suspended Calcium Carbonate

Apart from the retrieval of Primary Production, the MODIS sensor was utilized for the retrieval of monthly concentrations of Emilia huxleyi, coccoliths, diatomic chl and suspended inorganic carbon produced by Emilia huxleyi for the time period 2002-2010 (June-September) for the Arctic. For this purpose, a modified BOREALI algorithm has been employed for areas of Emilia huxleyi blooms (*Korosov et al., 2009; Petrenko et al., 2013*). The retrieved suspended inorganic carbon was compared to the suspended Calcium Carbonate of MICOM-HAMOCC-M. The 5364922 observations were interpolated to the MICOM-HAMOCC-M grid leading to a maximum of 34 month with observation for one MICOM-HAMOCC-M grid cell. Smaller numbers of observation-months are resulting from cloudiness and ice cover (*see Figure 13*).

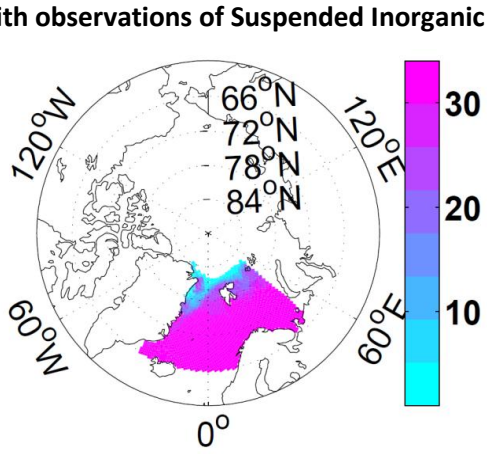

Figure 13: Number of months with data coverage of MODIS-Suspended Inorganic Carbon per MICOM-HAMOCC-M grid-cell for the time period 2002-2010.

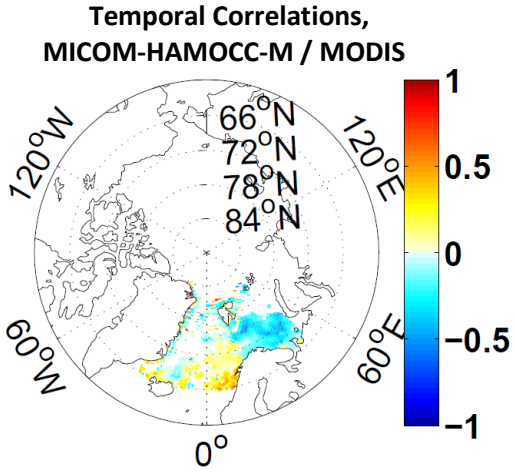

Figure 14: Temporal Correlations of the data-model-comparison between the data-product MODIS and the model MICOM-HAMOCC-M for the time period 2002-2010.

The results of the comparison between data-product and model show poor correlations for both spatial and temporal distributions (*see Figure 14*). These poor correlations are due to the fact that the comparison of concentrations of suspended $CaCO_3$ in the surface ocean from shell material belonging to the species Emiliania huxleyi (i.e. the available data-product) and the modelled tracer "suspended $CaCO_3$" is to be considered with care: The model includes all shell material of $CaCO_3$ forming organisms in one tracer (coccolithophoridae-shells, forminifera-shells, and also aragonitic shells - though the later are not explicitly accounted for in the model in general) and all formation of $CaCO_3$ shells is lumped together into an export flux of particulate inorganic carbon. Suspended $CaCO_3$ can re-enter the surface boxes of the model through circulation and mixing. Therefore, one can get at best a semi-quantitative hint on whether the model works through the observed data in our case. Nevertheless, this is some progress as one traditionally does not have any reliable information on biogenic $CaCO_3$ available in the upper ocean from observations. For a more straightforward comparison between model and observations, observation based estimates of export production rates of $CaCO_3$ would be needed.

3.3 Changes in the physical variables salinity and temperature

The arctic data-products for salinity and temperature were created by combining the data-products of LDEO, SOCAT, GLODAP, CARINA, and OWSM. GLODAP (GLobal Ocean Data Analysis Project; *Sabine et al., 2005*), CARINA (CARbon dioxide IN the Atlantic Ocean; *Key at al., 2010*), and OWSN (Ocean Weather Station M situated at 66°N, 2°E; *Skjelvan et al., 2008*) include measurements of temperature, salinity, alkalinity, dissolved inorganic carbon, and nutrients. For the GLODAP data-product were data of more than 50 individual cruises collected. The CARINA project includes data of 62 cruises/ campaigns in the Arctic Ocean and Nordic Seas, all ensuring consistency with the GLODAP data-product. While the datasets LDEO and SOCAT (both introduced in Section 3.3.1) contain only surface measurements, CARINA, GLODAP and OWSN include furthermore measurements of the deeper ocean. The collective data of all five data-products contains 810.276/ 686.844 observations (temperature/ salinity) for 1972-2011. In the realm of MICOM-HAMOCC-M this translates to a maximum of 80/ 76 months with data-coverage. Again, most of the grid cells have only a data-coverage of less than 10 months. Furthermore, the data-coverage is getting less in the deeper ocean.

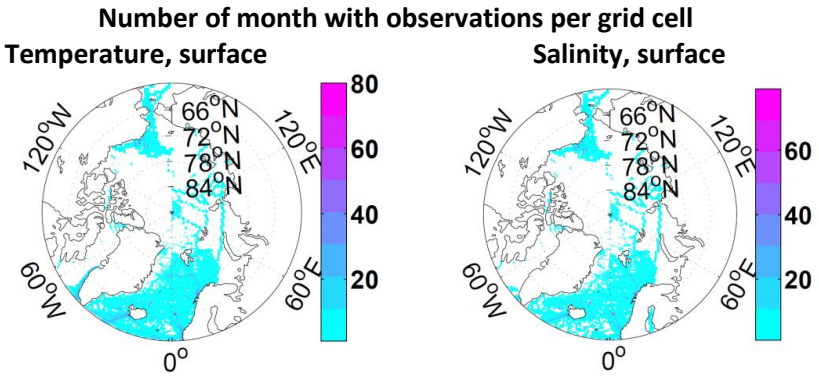

Figure 15: Number of months with SST (left) and SSS (right) data-coverage per MICOM-HAMOCC-M grid-cell for the time period 1972-2011.

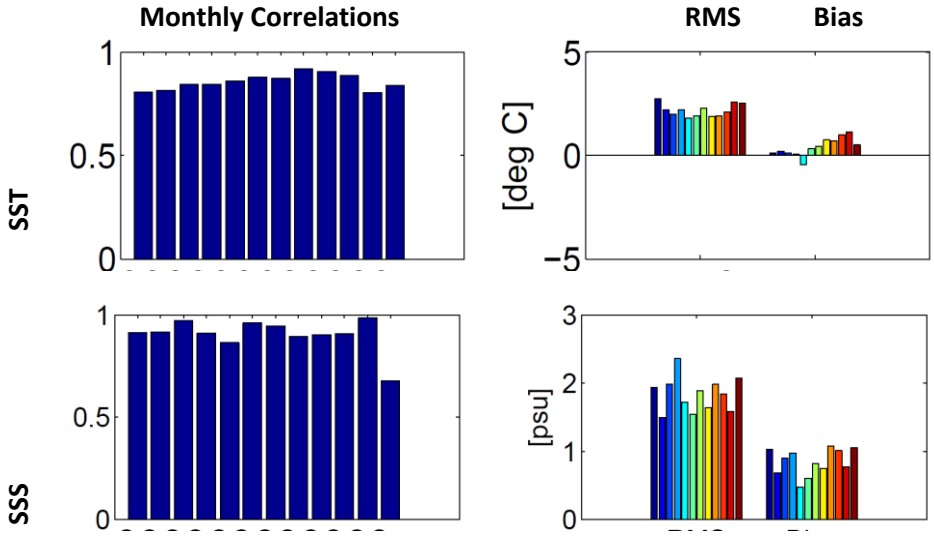

Figure 16: Monthly Correlations, Biases and Root Mean Square Errors of the spatial distribution for data product/model output for 1972-2011 (upper panel: SST, lower panel: SSS).

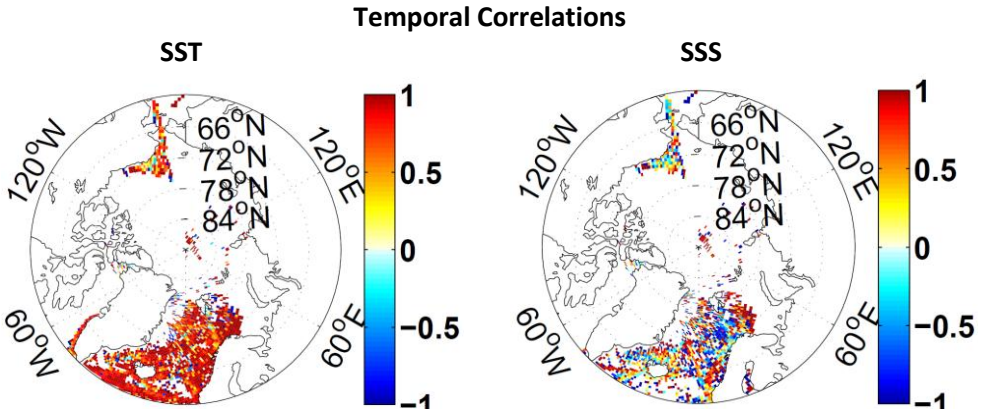

Figure 17: Temporal Correlations of the data-model-comparison between the data-product LDEO-SOCAT-GLODAP-CARINA-Station M and the model MICOM-HAMOCC-M for the time period 1972-2011 (upper panel: SST, lower panel: SSS).

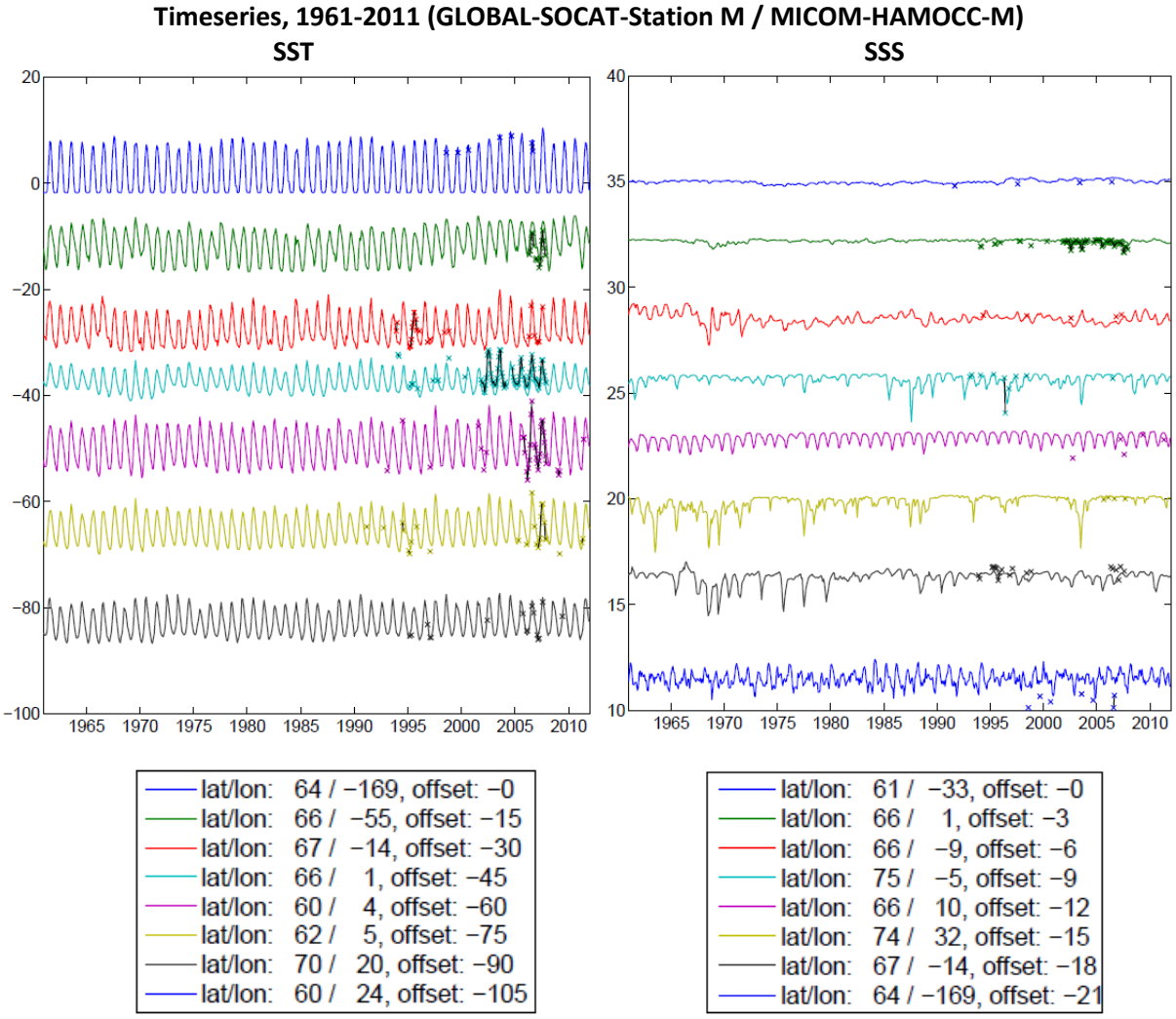

Figure 18: Selected Timeseries for 1961-2011 as modelled by MICOM-HAMOCC-M (colored lines, left panel: SST, right panel: SSS). SOCAT/GLODAP/Station M-records are marked by black lines. Associated offsets and coordinates are denoted in the lower panels.

The data-model comparison shows very good spatial correlations and moderate biases and root mean square errors for both sea surface temperature and sea surface salinity (*see Figure 16*), illustrating that the model performs very well. Considering temporal behaviour, model and data show very good agreement for temperature, but only poor agreement for salinity (*see Figure 17*). This feature is closely related to the fact the sea surface temperature has a relatively regular annual cycle (*see Figure 18*). Its temporal behaviour is therefore easier to model than the irregular annual cycle of salinity. Selected timeseries at different locations show that the trends of salinity and temperature are dependent on the location (*see Figure 18*). Figure 19 confirms this feature, illustrating that both salinity and temperature have a significant positive trend in the GIN seas and a negative trend north of Greenland (in 25-50m depth). While the positive trend in the GIN seas is visible as well in the deeper ocean, the negative trend north of Greenland cannot be established in the deeper ocean. Therefore it can be assumed that the negative trend north of Greenland is associated to ice melting. These trends are closely related to the sighted CO_2 uptake in Section 3.1.3.

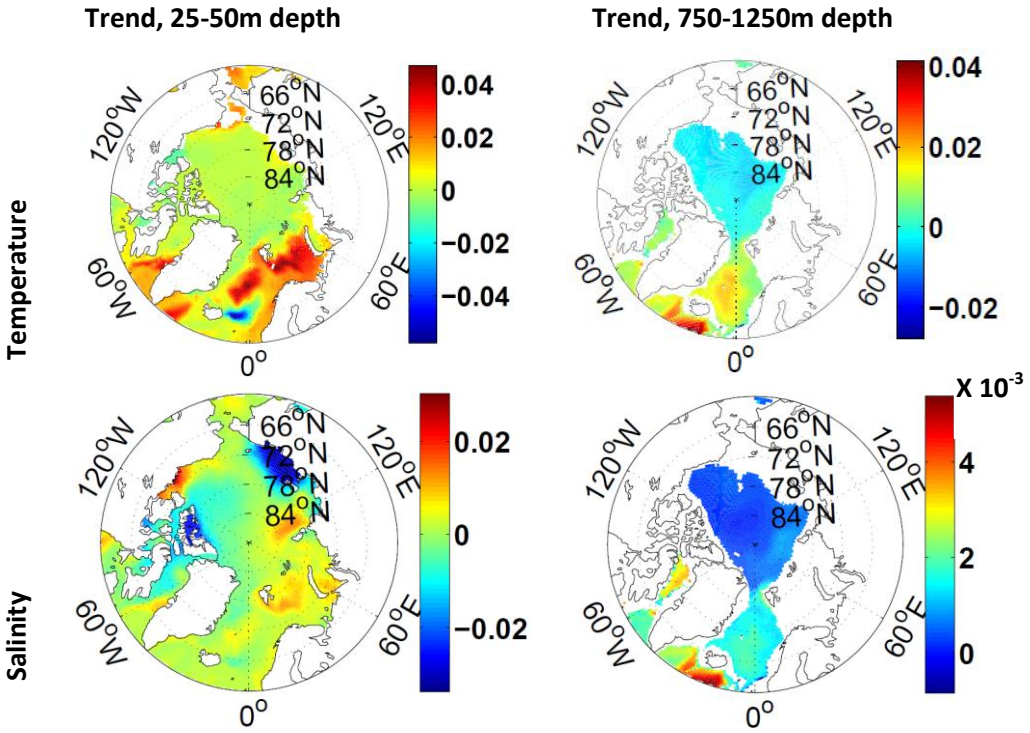

Figure 19: 50-year Trends (1961-2011) of Temperature and Salinity in two different depth levels as modelled by MICOM-HAMOCC-M.

3.4 Changes in the biogeochemical variables dissolved inorganic carbon, alkalinity, nitrate, phosphate, silicate, and oxygen

For the Arctic dataset of dissolved inorganic carbon (DIC), alkalinity, nitrate, phosphate, silicate, and oxygen, the data of CARINA, GLODAP and OWSM (all three data-products are described in Section 3.3) were collected north of 60°N. The newly created dataset consist of maximal 8.362 observations per variable (the number of observations is less for some of the variables) in the period of 1972-2007. This translates to a maximal data-coverage of 54 month per grid-cells. This maximum is only reached within one grid cell; most of the grid cells have a data-coverage of 1, 2 or 3 month. Figure 20 illustrates the data-coverage for phosphate surface data and the associated temporal correlations. For grid points with a data-coverage of only 1 month no temporal correlation was calculated. But even for grid cells with only 2 or 3 month of data-coverage a temporal correlation can be misleading (see Section 3.1.1). These grid-points do furthermore not allow for a validation of annual cycles. In order to gain a meaningful data-model-comparison, only the grid-point with 54 month of data-coverage is evaluated (OWSM is situated here). Due to the fact, that there are no measurements of oxygen included in the OWSM data-product, it is not possible to evaluate the model performance of oxygen.

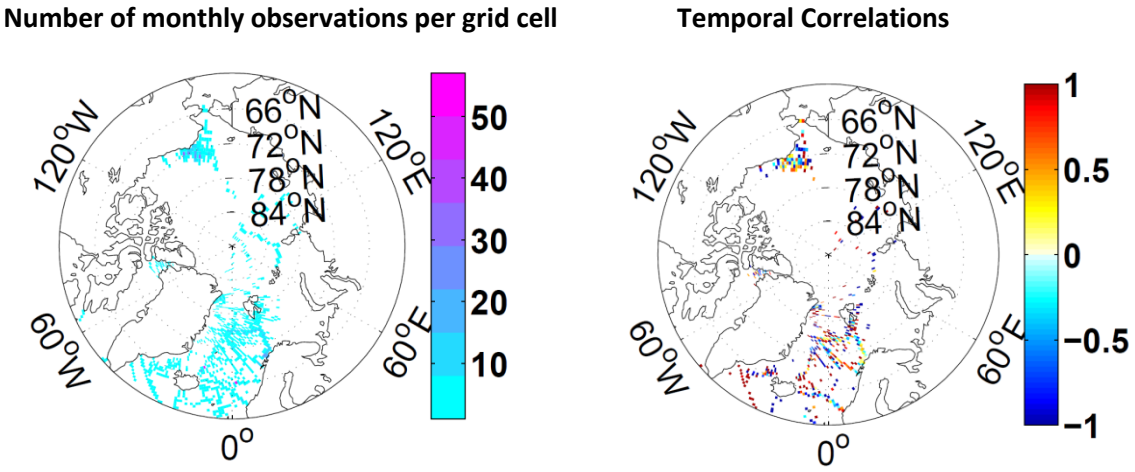

Figure 20: Number of months with phosphate surface data per MICOM-HAMOCC-M grid-cell (left panel) and associated temporal correlations of the data-model-comparison (right panel) for 1972-2011.

The data-model-comparison of OSWM and MICOM-HAMOCC-M shows that the model performs very well for Nitrate and Phosphate. Here, the temporal correlations are very high and the biases are very low (*see Figure 21*). While DIC and silicate show as well very high temporal correlations, their biases are larger, but still sufficiently small to ensure a good model performance. The alkalinity-values show a poor temporal correlation and a moderate bias. Given the irregular annual cycle of alkalinity and the level of difficulty for modelling alkalinity, the result is still acceptable. Based on these promising results, the modelled 50-year trend is evaluated. For silicate, DIC and alkalinity, the model shows positive, significant trends in the GIN seas (especially an accelerates increase in DIC, *see Figure 22*). T-tests show that the trends of nitrate and phosphate are not significant in the GIN seas. Phosphate, nitrate, silicate and alkalinity show furthermore negative trends in the region of the Beaufort gyre. These trends are significant for all variables.

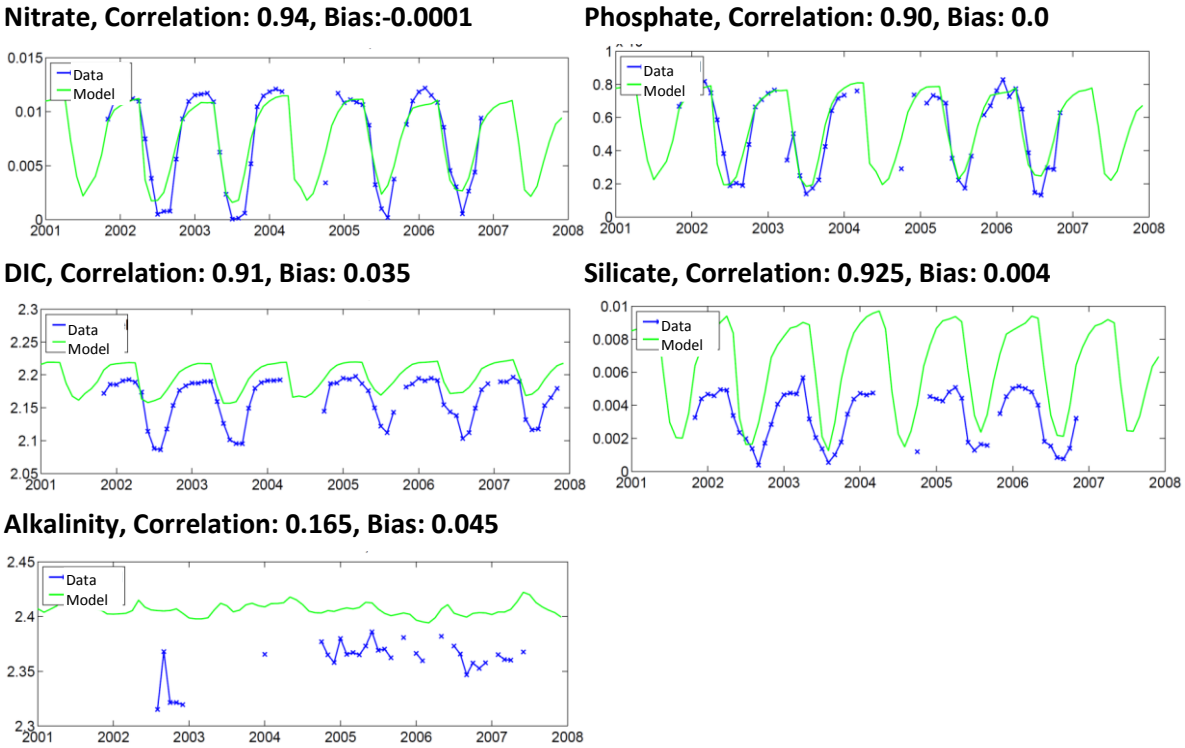

Figure 21: Selected Timeseries for 2001-2008 as modelled by MICOM-HAMOCC-M (green lines). Station M-records are marked by blue lines. Correlations and biases of the data-model-comparison are denoted on top of each panel.

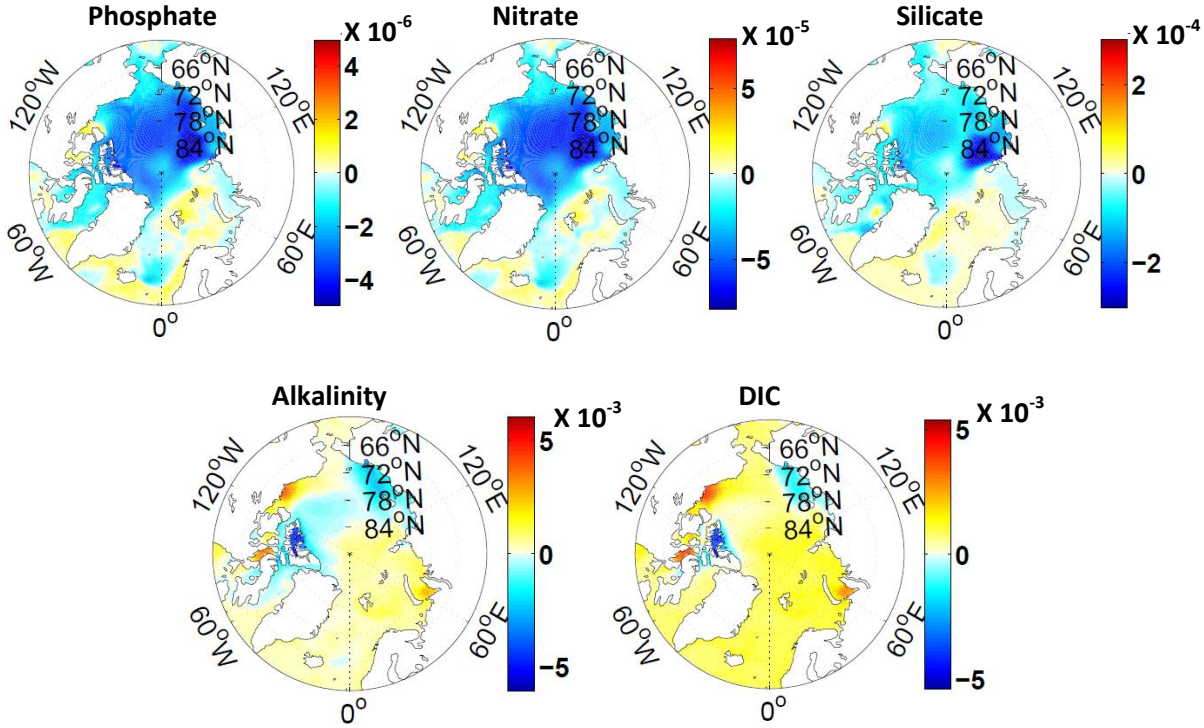

Figure 22: 50-year Trends (1961-2011) of Phosphate, Nitrate, Silicate, Alkalinity and Dissolved Inorganic Carbon (DIC) as modelled by MICOM-HAMOCC-M.

4 Summary

Despite the effort of MONARCH-A to collect and combine datasets of biogeochemical variables for the Arctic, a confident trend-analysis for key variables of the Arctic marine carbon cycle remains problematic. As Table 1 shows, the newly combined datasets contains no data for the period 1960-1970 and most of the data for the period 1970-1995 is only very sparse. Only recently (after 1995) more Arctic observations have become available. While this progress is very beneficial, it does allow for the calculation of 15-year-trends only. For variables with an irregular annual cycle such a short time span is not sufficient to identify significant tends. Furthermore, most of the regions are not sampled often enough, so that annual cycles are difficult to evaluate.

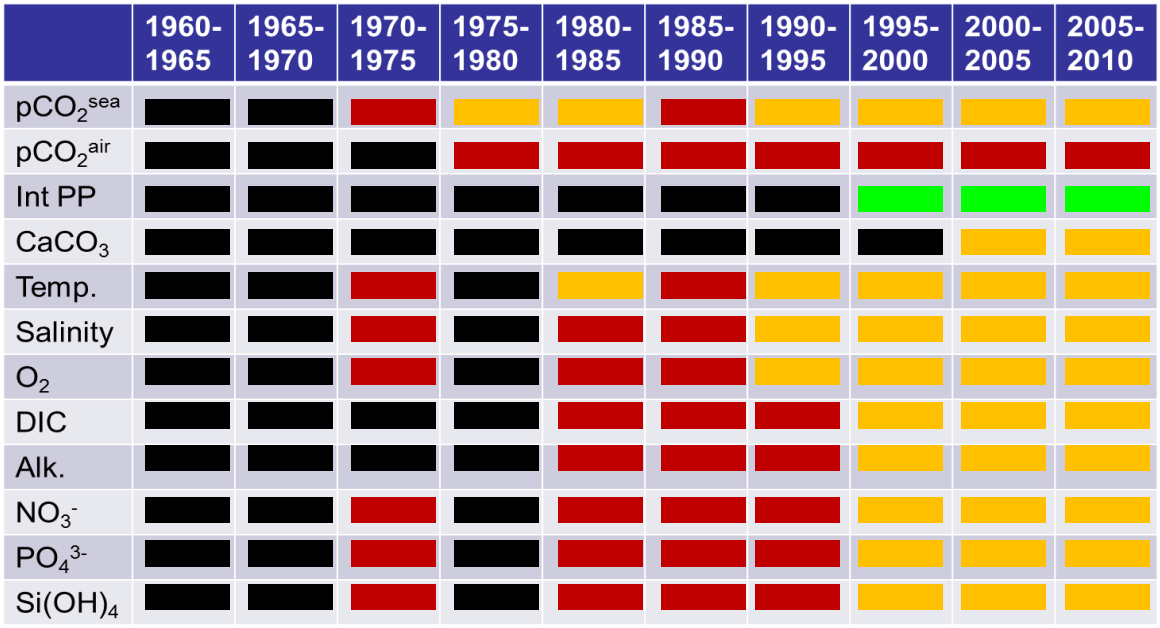

Table 1: Arctic data-availability of all considered variables for the time-period 1960-2010 (black: no data, red: data in less than 10 gridpoints, yellow: data covers less than 25% of the Arctic basin, green: data covers more than 70% of the Arctic basin).

With the newly combined dataset it was merely possible to confidently evaluate the model variables pCO_2^{atm} and Primary Production for the entire Arctic region. The dataset allows to confidently evaluating pCO_2^{sea}, temperature, and salinity in the Nordic seas. While DIC, alkalinity, phosphate, silicate, and nitrate can only be validated against data of the Ocean Weather Station M it can be assumed that the model performance is of approximately the same quality in the surrounding of the station. Finally, it is possible for all variables to confidently establish 50-year-trends in the GIN seas resulting in positive, significant trends for pCO_2^{sea}, pCO_2^{air}, temperature, salinity, DIC, alkalinity, and silicate. Due to the accelerated trend in pCO_2^{sea}, a recently stagnating CO_2-uptake can be found. This alarming finding is confirmed by the results of the run with free floating atmospheric CO_2.

Additional remark: The dissemination level of deliverable D3.3.2 was set to "PP" because some of the included observational data has not been published by its originators yet.

5 References

Aagaard, K., J.H. Swift, and E.C. Carmack (1985): Thermohaline circulation in the Arctic Mediterranean seas, *Journal of Geophysical Research – Oceans*, 90(NC3), 4833-4846.

Assmann, K.M., M. Bentsen, J. Segschneider, and C. Heinze (2010): An isopycnic ocean carbon cycle model, *Geoscientific Model Development,* 3, 143–167, www.geosci-model-dev.net/3/143/2010/

Behrenfeld, M. and P. Falkowski (1997): *Photosynthetic rates derived from satellite-based chlorophyll concentration,* Limnol. Oceanogr. 42(1): 1-20.

Behrenfeld, M., E. Boss, D. A. Siegel, and M. S. Donald (2005): *Carbon-based ocean productivity and phytoplankton physiology from space*, Global Biogeochemical Cycles. 19(GB1006), doi: 10.1029/2004GB002299.

Caldeira, K., and M.E. Wickett (2003): Anthropogenic carbon and ocean pH, *Nature*, 425, p. 365.

GLOBALVIEW-CO2 (2011): Cooperative Atmospheric Data Integration Project - Carbon Dioxide. CD-ROM, NOAA ESRL, Boulder, Colorado [Also available on Internet via anonymous FTP to ftp.cmdl.noaa.gov, Path: ccg/co2/GLOBALVIEW].

Guinotte, J.M., and V.J. Fabry (2008): Ocean Acidification and Its Potential Effects on Marine Ecosystems, *Annals of the New York Academy of Sciences,* 1134, 320–342.

Jeansson, E., A. Olsen, T. Eldevik, I. Skjelvan, A.M. Omar, S.K. Lauvset, J. E. Ø. Nilsen, R.G.J. Bellerby, T. Johannessen, and E. Falck (2011): The Nordic Seas carbon budget: Sources, sinks, and uncertainties, *Global Biogeochemical Cycles*, 25, GB4010.

Key, R. M., Tanhua, T., Olsen, A., Hoppema, M., Jutterström, S., Schirnick, C., van Heuven, S., Kozyr, A., Lin, X., Velo, A., Wallace, D. W. R., and Mintrop, L.: The CARINA data synthesis project: introduction and overview, *Earth Syst. Sci. Data*, 2, 105-121, doi:10.5194/essd-2-105-2010, 2010.

Korosov, A., D. Pozdnyakov, A. Folkestad, L. Pettersson, K. Sorensen, and R. Shuchman (2009): *Semi-empirical Algorithm for the Retrieval of Ecology-relevant Water Constituents in Various Aquatic Environments*, Algorithms, 2, pp. 470-497. doi:10.3390/a2010470.

Lundberg, L., and P.M. Haugan (1996): A Nordic Seas-Arctic Ocean carbon budget from volume flows and inorganic carbon data, *Global Biogeochemical Cycles*, 10, 3, 493-510.

Marra, J., C. Ho, C. Trees (2003): *An Alternative Algorithm for the Calculation of Primary Productivity from Remote Sensing Data,* LDEO Technical Report, #LDEO-2003-1, National Aeronautics and Space Administration Publ. 27 p.

Orr, J.C., V.J. Fabry, O. Aumont, L. Bopp, S.C. Doney, R.A. Feely, A. Gnanadesikan, N. Gruber, A. Ishida, F. Joos, R.M. Key, K. Lindsay, E.Maier-Reimer, R.Matear, P. Monfray, A. Mouchet, R.G. Najjar, G.-K. Plattner, K.B. Rodgers, C.L. Sabine, J.L. Sarmiento, R. Schlitzer, R.D. Slater, I.J. Totterdell, M.-F. Weirig, Y. Yamanaka, and A. Yool (2005): Anthropogenic ocean acidification over the twenty-first century and its impact on calcifying organisms, Nature, 437, 681-686.

Petrenko, D., Zabolotskikh, E., Pozdnyakov, D., and Karlin, L. (2012): Assessment of the adequacy of algorithms of the retrieval of primary production in the Arctic from satellite ocean colour data, *Scientific transactions of the Russian Hydrometeorological University*, 24, 137-162.

Petrenko, D., Pozdnyakov, D., Johannessen, J., Counillon, F., and Sychev, V. (2013): Satellite derived multi-year trend in primary production in the Arctic Ocean, *International Journal of Remote Sensing*, 3903-3937, doi:10.1080/01431161.2012.762698.

Petrenko, D., Zabolotsikh, E., Pozdnyakov, D., Counillon, F., and Karlin, L. (2013): Interannual variations of and trend in the production of inorganic carbon by coccolithophores in the Arctic during 2002-2010 as observed from space, *Earth research from space*, in press.

Pfeil, B., A. Olsen, D.C.E. Bakker et al. (2012): *A uniform, quality controlled, Surface Ocean CO2 Atlas (SOCAT),* submitted to Earth System Science Data (see *Earth Syst. Sci. Data Discuss*., 5, 735-780.

Sabine, C.L., R.A. Feely, N. Gruber, R.M. Kee, K. Lee, J.L. Bullister, R. Wanninkhof, C.S. Wong, D.W.R. Wallace, B. Tilbrook, F.J. Millero, T.-H. Peng, A. Kozyr, T. Ono, and A. Ríos (2004): The oceanic sink for anthropogenic CO2, *Science*, 305, 367-371.

Sabine, C. L., R. M. Key, A. Kozyr, R. A. Feely, R. Wanninkhof, F. J. Millero, T.-H. Peng, J. L. Bullister, and K. Lee (2005): *Global Ocean Data Analysis Project: Results and Data*, ORNL/CDIAC-145, NDP-083, Carbon Dioxide Information Analysis Center, Oak Ridge National Laboratory, U.S. Department of Energy, Oak Ridge, Tennessee, 110 pp

Skjelvan I., E. Falck, F. Rey, and S. B. Kringstad (2008): Inorganic carbon time series at Ocean Weather Station M in the Norwegian Sea, *Biogeosciences* 5(2), 549–560.

Steinacher, M., F. Joos, T.L. Frölicher, L. Bopp, P. Cadule, V. Cocco, S.C. Doney, M. Gehlen, K. Lindsay, J.K.Moore, B. Schneider, and J. Segschneider (2010): Projected 21st century decrease in marine productivity: a multi-model analysis, *Biogeosciences,* 7, 979-1005.

Steinacher, M., F. Joos, T.L. Frölicher, G.-K. Plattner, and S.C. Doney (2009): Imminent ocean acidification in the Arctic projected with the NCAR global coupled carbon cycle-climate model, *Biogeosciences*, 6, 515-533

Takahashi, T., S.C. Sutherland, and A. Kozyr (2012): *Global Ocean Surface Water Partial Pressure of CO_2 Database: Measurements Performed During 1957-2011 (Version 2011)*, ORNL/CDIAC-160, NDP-088(V2011), Carbon Dioxide Information Analysis Center, Oak Ridge National Laboratory, U.S. Department of Energy, Oak Ridge, Tennessee, doi: 10.3334/CDIAC/OTG.NDP088(V2011)**.**

Tjiputra, J.F., K. Assmann, M. Bentsen, I. Bethke, O.H. Otterå, C. Sturm, and C. Heinze (2010a): Bergen earth system model (BCM-C): Model description and regional climate-carbon cycle feedbacks assessment, Geoscientific Model Development, 3, 123–141.

Tjiputra, J.F., K. Assmann, and C. Heinze (2010b): Anthropogenic carbon dynamics in the changing ocean, *Ocean Science,* 6(3), 605-614.

Weiss, R.F. (1974): Carbon dioxide in water and seawater: The solubility of a non-ideal gas, *Marine Chemistry*, 2, 203-215.

END OF DOCUMENT